A Variable-Frequency ZVS Modulation for Four-Switch Buck+Boost Converters with Seamless Step-up/down Mode Transition

Guangyao Yu[1], Jianning Dong[1], Thiago Batista Soeiro[2], and Pavol Bauer[1]

[1]EEMCS, Delft University of Technology, Delft, The Netherlands
[2]EEMCS, University of Twente, Enschede, The Netherlands

***Abstract*—This paper introduces a variable-frequency zero voltage switching (ZVS) modulation strategy for the four-switch buck+boost converter with one operating pattern for the inductor current, i.e., three-segment inductor current modulation control. The proposed modulation scheme guarantees a smooth transition from step-up to step-down or from step-down to step-up operating modes without abrupt duty cycle or switching frequency change. Triangular current mode (TCM) ZVS control could be derived from this three-segment inductor current modulation strategy. Moreover, the controller design can be simplified compared with other multi-mode control methods. Experimental results were given to validate the modulation control strategy based on a $300-600$ V input, 400 V output, 3.3 kW prototype.**

***Index Terms*—zero voltage switching (ZVS), variable frequency, seamless transition, modulation.**

I. Introduction

Recently, more attention has been paid to the non-isolated four-switch buck+boost converter. This is due to its bi-directional power flow capability. Another reason is that it has both voltage boost and buck capabilities. For example, this converter has found a good application in the field of electric vehicles (EVs) charging due to its excellent performance for the wide operating range of input and output voltage values.

For the pursuit of power density design merit, which is usually realized by increasing switching frequency, soft switching technique has to be adopted to guarantee acceptable efficiency even with wide-bandgap (WBG) semiconductor devices [1], [2]. The soft-switched modulation strategies for the four-switch buck+boost converters can mainly be divided into two categories: fixed-frequency four-segment inductor current modulation [3]–[7] and variable-frequency modulation [1], [2], [8]–[10]. For both fixed- and variable-frequency zero voltage switching (ZVS) modulation, the basic principle is to utilize the inductor current during the dead time to charge and discharge the parasitic output capacitance C_{oss} of the MOSFET such that when the drain-source voltage damped to zero through the body diode conduction, the MOSFET can be turned on at zero voltage to reduce the switching losses.

This project has received funding from the Electronic Components and Systems for European Leadership Joint Undertaking under grant agreement No 876868. This Joint Undertaking receives support from the European Union's Horizon 2020 research and innovation programme and Germany, Slovakia, Netherlands, Spain, Italy.

For the fixed-frequency four-segment inductor current control, the optimization of the switching instant of the semiconductor device is complicated, besides, the selection of the inductance and switching frequency values are usually not covered in the literature. For variable-frequency modulation strategy [2], [8], TCM-ZVS control was extended to the transition mode, however, with this modulation, the root mean square (rms) value of the inductor current is not optimized, therefore, a sudden efficiency drop was observed, besides, an abrupt frequency and duty cycle change during the transition between different operating modes can also be found. In [11], all the possible variable-frequency ZVS modulation cases were studied in the buck-boost-type (transition) mode with duty cycle of d_1 being larger than d_2, it is found that the three-segment inductor current modulation is the most suitable solution with regard to inductor rms current reduction and convenient operation. Zhe Yu *et al.* proposed a novel variable-frequency ZVS control method in [10], however, both the analytical solution and experimentally recorded waveforms were missing. In [12], a single mode control strategy was proposed with a fixed duty cycle applied to S_1 (cf. Fig. 1), which, however, is a fixed-frequency hard-switched modulation.

In this paper, a variable-frequency ZVS modulation strategy with a seamless transition between step-down and step-up operating modes is presented and analyzed in detail with analytical solution, which, further more, will not compromise the inductor rms current compared with TCM-ZVS modulation. The proposed modulation strategy with feedback control is verified by experimental results.

II. Converter Operation

A. Voltage Gain of the Converter

The topology of the four-switch buck+boost converter is shown in Fig. 1.

In Fig. 1, S_1 and S_2 form the buck-type half-bridge circuit while S_3 and S_4 form the boost-type half-bridge. The pulse width modulation (PWM) signals applied to each half bridge are complementary. d_1 and d_2 are defined as the duty cycles of S_1 and S_4, respectively. The average voltage of terminals A and B with regard to the bottom-side dc-bus rail are

$$\bar{v}_A = d_1 V_1, \bar{v}_B = (1-d_2)V_2. \tag{1}$$

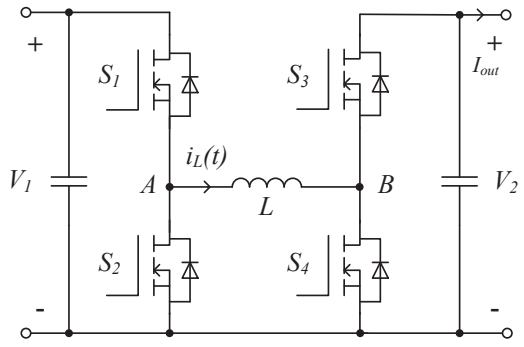

Fig. 1: Topology of the four-switch buck+boost converter.

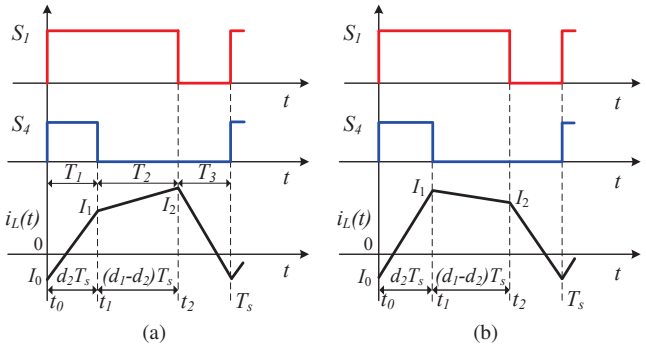

Fig. 2: Three-segment inductor current ZVS modulation. (a) $V_1 > V_2$. (b) $V_1 < V_2$.

Based on the volt-second balance law in quasi-steady-state operation for the inductor, the voltage gain can be derived as

$$G_v = \frac{V_2}{V_1} = \frac{d_1}{1-d_2}. \tag{2}$$

B. ZVS Modulation Control with Seamless Transition

The ZVS turn-on in a four-switch buck+boost converter requires the inductor current to be negative during the switching-on transition for S_1 and S_4, and to be positive while turning on S_2 and S_3. In this paper, the three-segment inductor current modulation adopted for the transition mode [11] will be extended to cover all the input and output voltage range with d_1 always being larger than d_2. The variable-frequency three-segment inductor current ZVS modulation is illustrated in Fig. 2.

In order to realize a smooth transition between step-up and step-down operating modes, the control variables of frequency and duty cycles are suggested to be continuous at the boundary [13], therefore, a control strategy of the duty cycles is proposed as below:

$$d_1 = \begin{cases} G_v(1-d_{\min}), G_v < 1 \\ d_{\max}, G_v \geq 1. \end{cases}, d_2 = \begin{cases} d_{\min}, G_v < 1 \\ 1 - \frac{d_{\max}}{G_v}, G_v \geq 1. \end{cases} \tag{3}$$

In (3), $d_{\min}$ and $d_{\max}$ are the minimum and maximum duty cycles respectively, and $d_{\min} + d_{\max} = 1$. As an illustration

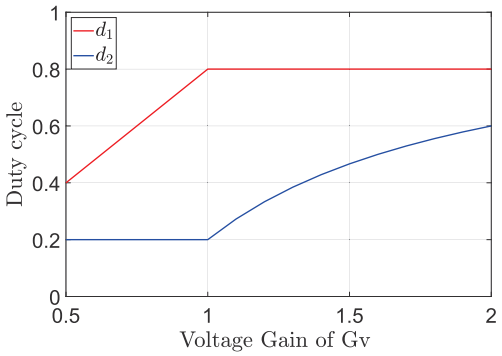

Fig. 3: An example of d_1 and d_2 values under different voltage gain.

example, Fig. 3 shows the duty cycle of d_1 and d_2 under voltage gain G_v between 0.5 and 2.

In Fig. 2, for both step-up and step-down operating cases, the inductor current expression can be written as below with $t_0 = 0$,

$$i_L(t) = \begin{cases} I_0 + \frac{V_1}{L}t, 0 < t \leq t_1 \\ i_L(t_1) + \frac{V_1 - V_2}{L}(t - t_1), t_1 < t \leq t_2 \\ i_L(t_2) - \frac{V_2}{L}(t - t_2), t_2 < t \leq T_s. \end{cases} \tag{4}$$

In (4), $T_1 = t_1 - t_0 = d_2T_s$, $T_2 = t_2 - t_1 = (d_1 - d_2)T_s$, T_s is the switching period. Since the power is only transferred when S_3 is on, so, the average output current is

$$I_{out} = \frac{I_1 + I_2}{2}(d_1 - d_2) + \frac{I_2 + I_0}{2}(1 - d_1). \tag{5}$$

Based on (2), (4) and (5), the expression for switching frequency is derived as

$$f_s = \frac{\frac{V_1}{2}[d_1(1-d_1) + d_2(d_1 - d_2)]}{L[I_{out} - I_0(1-d_2)]}. \tag{6}$$

I_0 is set as a fixed negative value for the variable-frequency ZVS modulation. By substituting (6) into (4), one can get

$$I_1 = \frac{2d_2I_{out} + [(1-d_1)(d_1 - d_2) + d_2(d_2 - 1)]I_0}{d_1(1-d_1) + d_2(d_1 - d_2)}. \tag{7}$$

$$I_2 = \frac{2d_1(1-d_1)I_{out} + (1-d_2)[d_2(d_1 - d_2) + d_1(d_1 - 1)]I_0}{(1-d_2)[d_1(1-d_1) + d_2(d_1 - d_2)]}. \tag{8}$$

For (6), (7) and (8), when I_0 becomes zero, then the corresponding equations for the critical conduction mode (CRM) could also be derived directly. Based on (7) and (8), the current values of I_1 and I_2 are independent of inductance. According to [11], the inductor current rms value is also independent of inductance, which is

$$I_{Lrms} = \sqrt{I_{Lrms1}^2 + I_{Lrms2}^2 + I_{Lrms3}^2}. \tag{9}$$

I_{Lrms1}, I_{Lrms2} and I_{Lrms3} are the rms values of each segment of the inductor current, and they can be expressed as

$$I_{Lrms1} = \sqrt{d_2\frac{I_0^2 + I_1^2 + I_0I_1}{3}}, I_{Lrms2} = \sqrt{(d_1 - d_2)\frac{I_1^2 + I_2^2 + I_1I_2}{3}},$$
$$I_{Lrms3} = \sqrt{(1-d_1)\frac{I_2^2 + I_0^2 + I_2I_0}{3}}. \tag{10}$$

C. Relations with TCM-ZVS Modulations

Triangular current mode (TCM) ZVS modulation for typical buck, boost and buck-boost modes can all be derived from the three-segment inductor current modulation described above simply by applying corresponding duty cycles to the derived formulas of (6), (7) and (8). Assuming I_0 and I_1 to be the valley and peak inductor current value for TCM-ZVS modulation respectively. The rms value of the inductor current for TCM-ZVS buck, boost and buck-boost modulations can all be expressed as

$$I_{Lrms} = \sqrt{\frac{1}{3}(I_0^2 + I_1^2 + I_0 I_1)}. \tag{11}$$

1) TCM-ZVS Buck Mode: In this mode, $d_2 = 0$ and $d_1 = \frac{V_2}{V_1}$, therefore,

$$f_s = \frac{V_1 d_1 (1 - d_1)}{2L(I_{out} - I_0)}, I_1 = 2I_{out} - I_0. \tag{12}$$

2) TCM-ZVS Boost Mode: In this mode, $d_1 = 1$ and $d_2 = 1 - \frac{V_1}{V_2}$, therefore,

$$f_s = \frac{V_1 d_2 (1 - d_2)}{2L[I_{out} - I_0(1 - d_2)]}, I_1 = \frac{2I_{out}}{1 - d_2} - I_0. \tag{13}$$

3) TCM-ZVS Buck-Boost Mode : In this mode, $d = d_1 = d_2 = \frac{V_2}{V_1 + V_2}$, therefore,

$$f_s = \frac{V_1 d(1 - d)}{2L[I_{out} - I_0(1 - d)]}, I_1 = \frac{2I_{out}}{1 - d} - I_0. \tag{14}$$

D. Inductor RMS Current and Switching Frequency

The inductor rms current comparison between TCM-ZVS and the proposed modulation strategy is shown in Fig. 4 based on the parameters from the laboratory prototype. Herein, $V_1 = 300 - 600$ V, $V_2 = 400$ V, $P_o = 3.3$ kW. The duty cycles are between 0.1 and 0.9.

In Fig. 4, the TCM-ZVS mode is subdivided into TCM-ZVS buck, boost and buck-boost modes as described previously. It can be seen from Fig. 4, the inductor rms current at $d_{max} = 0.9$ is in fact even smaller than both TCM-ZVS buck and boost mode operation. When $d_{max} = 0.8$, the current rms value is a bit larger than TCM-ZVS buck or boost mode operation. The selection of I_0 is explained in Section III.

Fig. 5 shows the switching frequency at 3.3 kW and 500 W respectively. As expected, the frequency is continuous at the voltage gain boundary.

Due to the high switching frequency at low power condition, a frequency limiter is adopted. In this paper, the switching frequency is set between 20 kHz and 160 kHz.

E. Closed-loop Control Diagram

A closed-loop control is proposed for the modulation strategy, which is shown in Fig. 6 based on the derived equations of (3) and (6). Compared with multi-mode operation [11], [14], the hysteresis comparison function between the input and output voltage can also be avoided due to the continuity of control variables.

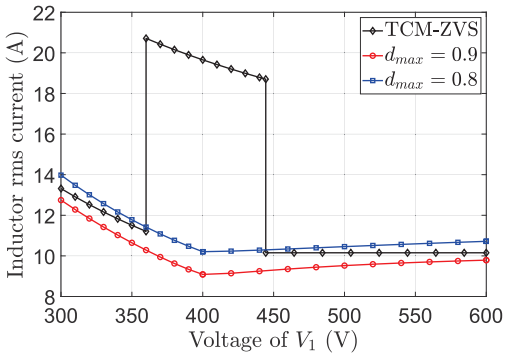

Fig. 4: Inductor rms current comparison at 3.3 kW with I_0 being -2 A.

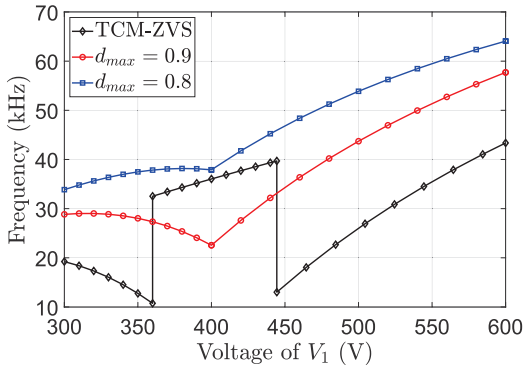

(a)

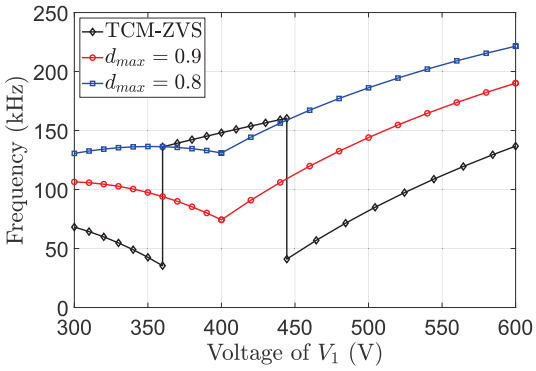

(b)

Fig. 5: Switching frequency with $L = 150$ μH and $I_0 = -2$ A. (a) 3.3 kW. (b) 500 W.

III. Experimental Verification

The converter prototype is shown in Fig. 7. Each single switch was composed of three parallel-connected silicon carbide (SiC) MOSFETs of G3R75MT12J from GeneSiC semiconductor to increase its current rating capability. The inductor was made with N87 material on PM 74/59 core. The inductance and equivalent resistance is given in Table I, which was measured by Agilent 4294A precision impedance analyzer. During experiments, the inductance was selected as 155.5 μH. As a key parameter, the switched ZVS current of

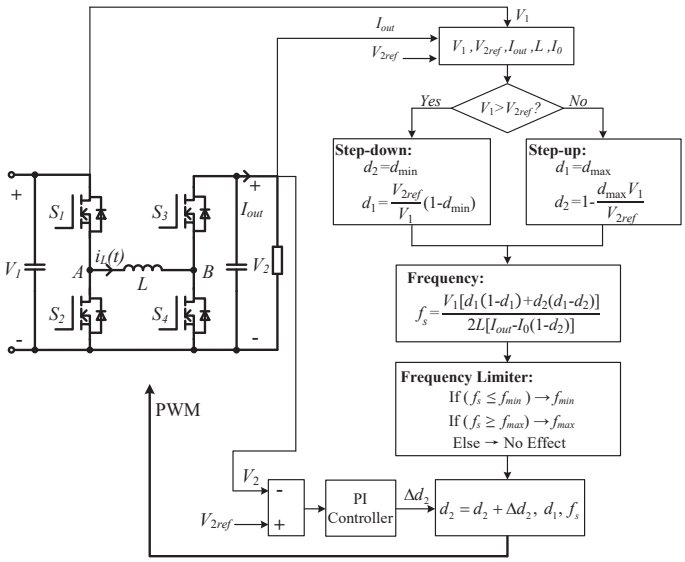

Fig. 6: Closed-loop control diagram.

I_0 can be estimated by (15) as

$$|I_0| \geq \frac{2C_{oss}\max\{V_1, V_2\}}{t_{dead}}. \tag{15}$$

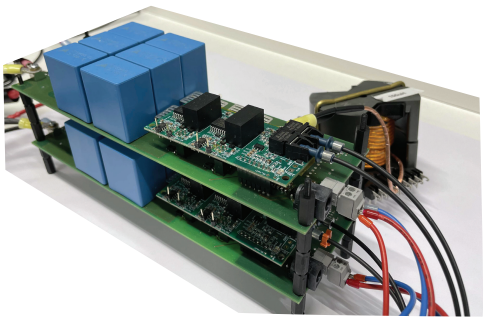

Fig. 7: Four-switch buck+boost converter prototype.

TABLE I: Inductance and equivalent resistance of the inductor

Frequency (kHz)	20	60	100	140	160
L (μH)	155.51	155.53	155.48	155.53	155.70
R_s (mΩ)	49.5	99.5	144.7	205.9	283.0

In (15), C_{oss} is the lump equivalent output capacitance of the MOSFET and t_{dead} is the dead time. Herein, I_0 is chosen as -2 A and the dead time is 300 ns.

A. Steady State Operation

The experimental oscilloscope waveforms are given in Fig. 8 when the input voltage is 300 V, 400 V and 600 V respectively at 3.3 kW power level. The value of d_{max} is chosen as 0.8.

As it can be seen from Fig. 8, at switching transient when the inductor current is at its lowest value, V_B dropped to zero while V_A reached to the input voltage value when turning on

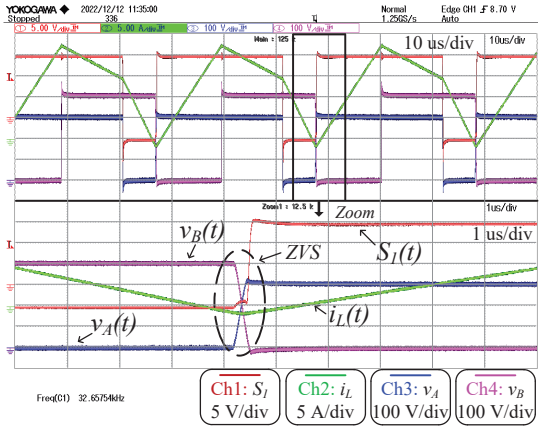

(a)

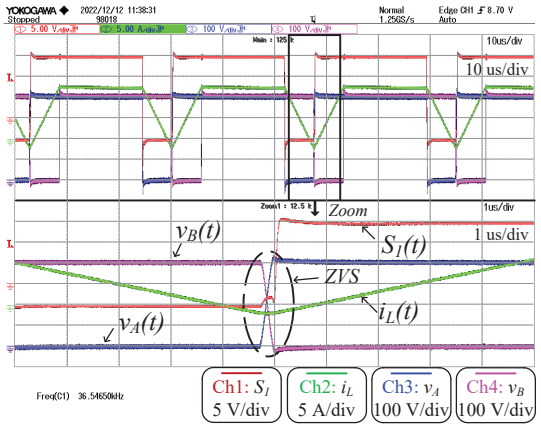

(b)

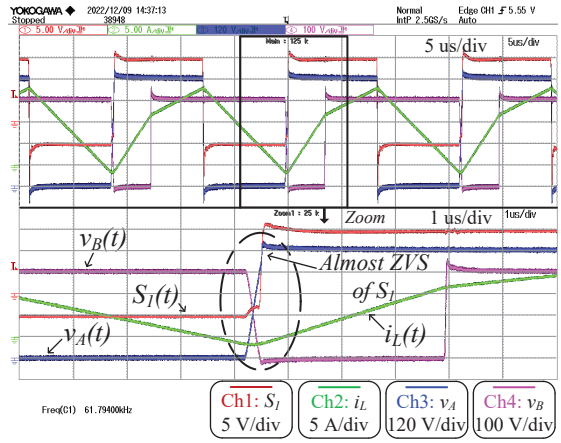

(c)

Fig. 8: Measured waveforms and efficiency at $V_1 = 300$, 400 and 600 V, $P_o = 3.3$ kW, $d_{max} = 0.8$, $V_2 = 400$ V. The switching frequency is calculated based on (6). $S_1(t)$ is the gate-source voltage of S_1, $i_L(t)$ is the inductor current, $v_A(t)$ and $v_B(t)$ are the voltage potentials of terminals A and B relative to the bottom-side dc-bus rail shown in Fig. 1. (a) $V_1 = 300$ V. (b) $V_1 = 400$ V. (c) $V_1 = 600$ V.

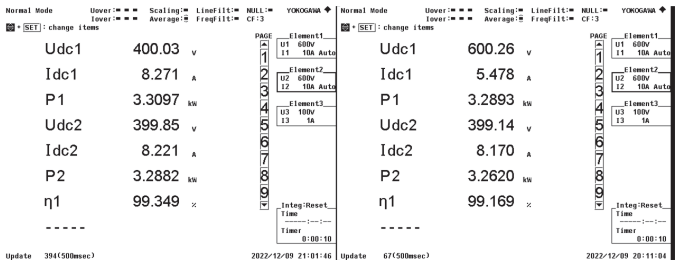

Fig. 9: Measured efficiency from Yokogawa WT500 power analyzer. Udc1, Idc1 and P1 are the DC bus voltage, current and delivered active power values respectively from input side while Udc2, Idc2 and P2 are the DC bus voltage, current and delivered active power values respectively from the output side. The prototype efficiency is defined as $\eta 1 = \frac{P2}{P1}$.

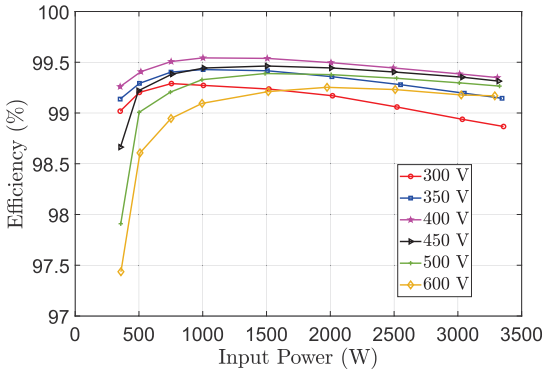

Fig. 10: Measured efficiency at different operating input voltage and power values with $V_2 = 400$ V and $d_{max} = 0.8$.

S_4 and S_1. For 600 V input, which is the hardest case to realize ZVS turn-on of S_1, V_A almost reached V_1 when S_1 was turned on, therefore, it can be concluded that the ZVS turn-on for the four switches was achieved simultaneously.

Fig. 9 shows the efficiency measured by Yokogawa WT500 power analyzer at 3.3 kW when input voltage is 400 V and 600 V respectively. Efficiency measured at different operating points is shown in Fig. 10, which, covers a power range between 350 and 3300 W, as it can be seen, the efficiency remains at a relatively high value in a wide operational range.

B. Transition Operation under Constant Power

The transient experiment was carried out under a constant power of 2 kW based on control logic from Fig. 6, the input voltage first decreased from 425 V to 375 V, after another period of 1 s, it rose from 375 V to 425 V to cover both transition cases from voltage step-down to step-up and voltage step-up to step-down. The result is given in Fig. 11.

As it can be seen from Fig. 11, the converter could operate smoothly (i.e., display a seamless transition) as expected when it crosses the voltage gain boundary, which proves the operating principles and advantages of the proposed modulation strategy for the four-switch buck+boost converter.

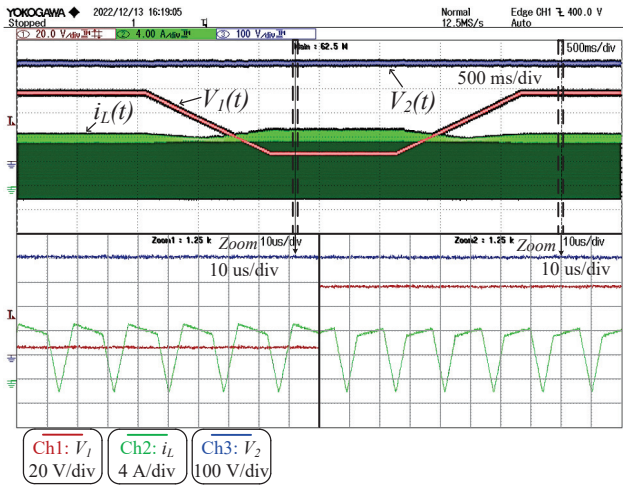

Fig. 11: Experiments of transition operation. $V_1 = 425 - 375 - 425$ V, $V_2 = 400$ V, $d_{max} = 0.8$, $P_o = 2$ kW, $I_0 = -2$ A.

IV. Conclusion

A variable-frequency zero voltage switching (ZVS) modulation strategy for the four-switch buck+boost converters featuring seamless step-up/down mode transition with analytical solution has been introduced in this paper. One operating pattern of three-segment inductor current was applied to the converter operation for all the working conditions. Due to the continuity of the control variables of duty cycles and switching frequency, the converter can realize a smooth transition at the boundary of voltage step-up and step-down. Finally, The modulation strategy was verified by experiments.

References

[1] A. J. Hanson, R. S. Yang, S. Lim and D. J. Perreault, "A soft-switched high frequency converter for wide voltage and power ranges," 2016 IEEE International Telecommunications Energy Conference (INTELEC), 2016, pp. 1-8, doi: 10.1109/INTLEC.2016.7749103.

[2] K. Kruse, M. Elbo and Z. Zhang, "GaN-based high efficiency bidirectional DC-DC converter with 10 MHz switching frequency," 2017 IEEE Applied Power Electronics Conference and Exposition (APEC), 2017, pp. 273-278, doi: 10.1109/APEC.2017.7930705.

[3] Vinciarelli, Patrizio. "Buck-boost DC-DC switching power conversion." U.S. Patent No. 6,788,033. 7 Sep. 2004.

[4] S. Waffler and J. W. Kolar, "A Novel Low-Loss Modulation Strategy for High-Power Bidirectional Buck ++ Boost Converters," in IEEE Transactions on Power Electronics, vol. 24, no. 6, pp. 1589-1599, June 2009, doi: 10.1109/TPEL.2009.2015881.

[5] L. Tian, X. Wu, C. Jiang and J. Yang, "A Simplified Real-Time Digital Control Scheme for ZVS Four-Switch Buck–Boost With Low Inductor Current," in IEEE Transactions on Industrial Electronics, vol. 69, no. 8, pp. 7920-7929, Aug. 2022, doi: 10.1109/TIE.2021.3104616.

[6] Z. Zhou, H. Li and X. Wu, "A Constant Frequency ZVS Control System for the Four-Switch Buck–Boost DC–DC Converter With Reduced Inductor Current," in IEEE Transactions on Power Electronics, vol. 34, no. 7, pp. 5996-6003, July 2019, doi: 10.1109/TPEL.2018.2884950.

[7] Q. Liu, Q. Qian, M. Zheng, S. Xu, W. Sun and T. Wang, "An Improved Quadrangle Control Method for Four-Switch Buck-Boost Converter With Reduced Loss and Decoupling Strategy," in IEEE Transactions on Power Electronics, vol. 36, no. 9, pp. 10827-10841, Sept. 2021, doi: 10.1109/TPEL.2021.3064074.

[8] Z. Yu, H. Kapels and K. F. Hoffmann, "High Efficiency Bidirectional DC-DC Converter with Wide Input and Output Voltage Ranges for Battery Systems," Proceedings of PCIM Europe 2015; International Exhibition and Conference for Power Electronics, Intelligent Motion, Renewable Energy and Energy Management, 2015, pp. 1-8.

[9] Z. Yu, H. Kapels and K. F. Hoffmann, "Extreme High Efficiency Non-Inverting Buck-Boost Converter for Energy Storage Systems," PCIM Europe 2016; International Exhibition and Conference for Power Electronics, Intelligent Motion, Renewable Energy and Energy Management, 2016, pp. 1-8.

[10] Z. Yu, H. Kapels and K. F. Hoffmann, "A novel control concept for high-efficiency power conversion with the bidirectional non-inverting buck-boost converter," 2016 18th European Conference on Power Electronics and Applications (EPE'16 ECCE Europe), 2016, pp. 1-10, doi: 10.1109/EPE.2016.7695309.

[11] G. Yu, J. Dong, T. B. Soeiro, G. Zhu, Y. Yao and P. Bauer, "Three-Mode Variable-Frequency ZVS Modulation for Four-Switch Buck+Boost Converters With Ultra-high Efficiency," in IEEE Transactions on Power Electronics, doi: 10.1109/TPEL.2022.3231969.

[12] Y. Wang, J. Lan, X. Huang, T. Fang, X. Ruan and M. Dong, "An Improved Single-mode Control Strategy Based on Four-switch Buck-Boost Converter," 2020 IEEE Applied Power Electronics Conference and Exposition (APEC), New Orleans, LA, USA, 2020, pp. 320-325, doi: 10.1109/APEC39645.2020.9124612.

[13] L. Tian, X. Wu, C. Jiang and J. Yang, "A Simplified Real-Time Digital Control Scheme for ZVS Four-Switch Buck–Boost With Low Inductor Current," in IEEE Transactions on Industrial Electronics, vol. 69, no. 8, pp. 7920-7929, Aug. 2022, doi: 10.1109/TIE.2021.3104616.

[14] X. Ren, X. Ruan, H. Qian, M. Li and Q. Chen, "Three-Mode Dual-Frequency Two-Edge Modulation Scheme for Four-Switch Buck–Boost Converter," in IEEE Transactions on Power Electronics, vol. 24, no. 2, pp. 499-509, Feb. 2009, doi: 10.1109/TPEL.2008.2005578.